Journal of Geophysical Research: Atmospheres

RESEARCH ARTICLE
10.1029/2018JD029003

Analysis of Climate Trends and Leading Modes of Climate Variability for MENA Region

Muhammad Mubashar Dogar[1] and **Tomonori Sato**[2]

[1]Global Change Impact Studies Centre, Ministry of Climate Change, Islamabad, Pakistan, [2]Faculty of Environmental Earth Science, Hokkaido University, Sapporo, Japan

Key Points:
- MENA region is very sensitive to the changes induced by the internal and external climate forcings
- This paper focuses on the importance of trend in data and leading climate modes that play significant role in shaping MENA climate
- Both the model and the observations indicate that positive phase of NAO and ENSO significantly cools central parts of MENA in winter

Correspondence to:
M. M. Dogar,
mubashardogar@yahoo.com

Citation:
Dogar, M. M., & Sato, T. (2018). Analysis of climate trends and leading modes of climate variability for MENA region. *Journal of Geophysical Research: Atmospheres*, *123*, 13,074–13,091. https://doi.org/10.1029/2018JD029003

Received 14 MAY 2018
Accepted 31 OCT 2018
Accepted article online 5 NOV 2018
Published online 4 DEC 2018

Author Contributions:
Formal analysis: Muhammad Mubashar Dogar
Writing – review & editing: Muhammad Mubashar Dogar, Tomonori Sato

Abstract The Middle East and North Africa (MENA), primarily the Arabian Peninsula (AP), is a region where the rate of mean surface temperature rise per decade is among the highest globally known during the recent past. Moreover, MENA regional climate is very sensitive to internal and external climate drivers. Therefore, it is of significant practical importance to analyze MENA sensitivity to climate trends as well as leading variability modes such as El Niño Southern Oscillation (ENSO), North Atlantic Oscillation (NAO), and Indian summer monsoon (ISM). Using multiple regression technique on observations and the high-resolution atmospheric model output, this study investigates the role of climate trends and leading circulation modes such as NAO, ENSO, and ISM in inducing temperature and precipitation variability in MENA region for the period 1979–2008. Our results show substantial regional temperature and precipitation responses of ENSO, NAO, and ISM over MENA. Both the model and the observations indicate that positive phase of NAO and ENSO significantly cools central parts of MENA, in particular, the AP in winter. However, in boreal summer, the warm ENSO phase produces significant warming and drying over the tropical region. The strengthening (weakening) of ISM suggests cooling (warming) and wetting (drying) over MENA rain-belt region. Moreover, ISM induces a dipole precipitation structure over the tropics caused by Intertropical Convergence Zone shift and associated cloud distribution. High-resolution atmospheric model slightly underestimates NAO and ENSO winter cooling over the AP; however, overall patterns are well reproduced. The conducted analysis sheds light on the internal mechanisms of MENA climate variability.

1. Introduction

The Middle East and North Africa (MENA), primarily the Arabian Peninsula (AP), is a region where the rate of mean surface temperature rise per decade is among the highest globally known during the recent past (Almazroui et al., 2012; AlSarmi & Washington, 2011, 2013; Croitoru & Piticar, 2012; del Río et al., 2013; Hansen et al., 2010; Zhang et al., 2005). Earlier studies have shown that the MENA region is very sensitive to internal and external climate forcings (Bangalath & Stenchikov, 2015; Dogar, 2018; Dogar, Kucharski, et al., 2017; Dogar, Stenchikov, et al., 2017; Haywood et al., 2013; Osipov et al., 2016; Stenchikov & Dogar, 2012). Several past studies have discussed the importance of different leading modes of variabilities such as North Atlantic Oscillation (NAO; Abualnaja et al., 2015; Athar, 2014; Barlow et al., 2016; Hurrell, 1995), El Niño Southern Oscillation (ENSO; Dogar, Kucharski, et al., 2017; Kumar et al., 2016), and Indian summer monsoon (ISM); however, there is barely any attempt conducted so far in which the sensitivity of MENA to these leading predictors is explored in detail. Using comprehensive statistical approaches, Zhang et al. (2005) examined in detail the trends in temperature and precipitation indices for Middle East region. Some recent studies have analyzed the response of AP region to ENSO or NAO forcings (see, e.g., Abid et al., 2018; AlSarmi & Washington, 2011, 2013; Kumar et al., 2016; Sandeep & Ajayamohan, 2018). Nevertheless, the impact of the leading climate factors on the MENA region is marginally explored, and therefore, further studies to improve our understanding are warranted. Hence, the aim of this study is to revisit and better understand the impact of leading modes of variabilities that influence MENA climate together with the assessment of climatic contribution of temperature and precipitation trends in winter (December to February [DJF]) and summer (June to August [JJA]) season. For this purpose we will make use of regression analysis, which is widely used to study the global and regional climatic impact of large-scale climate drivers (Dogar, Stenchikov, et al., 2017; Iles & Hegerl, 2017; Randel, 2010; Yu & Zhou, 2004). The regression analysis is employed on the output from high-resolution global climate model together with state-of-the-art observational data to better analyze the leading variability modes and their regional impacts over MENA region.

This study will surely help the policy makers to get prepared about the climatic impact of such leading predictors. To the best of our knowledge, this study is an antecedent and first of its kind in which a very fine resolution global climate model is used to uncover the regional climatic mechanisms of MENA and its sensitivity to leading modes of variabilities. The main questions that are discussed in this paper are as follows: (1) What is the role of temperature and precipitation trends over MENA region? (2) How the leading modes of variabilities (ENSO, NAO, and ISM) affects MENA climatic regime?

The rest of the paper is organized as follows. In section 2 we have discussed the model, data, and methodology used in the study. Subsection 2.1 describes model, experimental setup, and the observational data used in the study. Subsection 2.2 explains the methodology that includes multiple linear regression (MLR) technique and selection of leading climate modes of variability for MENA (subsection 2.2.2). In section 3, results and discussion are presented, in which we discuss climate trends and the leading modes of variabilities along with their climatic impacts over MENA. In the last section, summary and conclusions of the study are presented.

2. Model, Data, and Methodology

2.1. Model Description, Experimental Setup, and Data

For the study of temperature and precipitation trend in data and the impact of leading teleconnection modes in the MENA region, we employ the Geophysical Fluid Dynamics Laboratory (GFDL)'s global high-resolution atmospheric model, HiRAM. It is based on version 2 of the GFDL Atmospheric Model (AM2; Anderson et al., 2004), with improved horizontal and vertical resolutions. It has 32 vertical layers instead of 24 that reach up to 10 hPa, to better simulate the processes in the lower stratosphere and coupling with the troposphere. It has simplified parameterizations for moist convection and large-scale stratiform cloudiness. The relaxed Arakawa-Schubert convective closure scheme used in AM2 has been replaced by a shallow convective parameterization scheme (Bretherton et al., 2004; Moorthi & Suarez, 1992). HiRAM model uses a comparatively new cubed-sphere finite-volume dynamic core (Putman & Lin, 2007) and a prognostic cloud scheme with a subgrid scale distribution of total water and multispecies tropospheric aerosol climatology that is based on the Model for Ozone and Related Chemical Tracers (Horowitz et al., 2003). HiRAM retains the surface flux, land surface, boundary layer, radiative transfer modules, gravity wave drag, and large-scale cloud microphysics of AM2 (Anderson et al., 2004; Zhao et al., 2009). The land model, LM3, used by HiRAM, includes soil sensible and latent heat storage, groundwater storage, and stomata resistance (Malyshev et al., 2015).

The shortwave (SW) radiation algorithm of HiRAM model follows Freidenreich and Ramaswamy (1999). The SW spectrum ranges from 0.17 to 4.0 μm and is divided into 25 bands: 10 bands in the near infrared region, 4 bands in the visible region, and 11 bands in the ultraviolet region. The SW radiation code includes absorption by H_2O, CO_2, O_3, O_2, and Rayleigh scattering. The longwave radiation code follows a modified form of the simplified exchange approximation (Schwarzkopf & Ramaswamy, 1999). It accounts for the absorption and emission by the principal gases present in the atmosphere, including H_2O, CO_2, N_2O, O_3, and CH_4, and the halocarbons, CFC-11, CFC-12, CFC-113, and HCFC-22. Aerosols and clouds are treated as absorbers in the longwave radiation code, with nongray absorption coefficients specified in the eight spectral bands of the transfer scheme, following the methodology explained in Ramachandran et al. (2000). A detailed documentation of the HiRAM model and a list of recent publications can be found at http://www.gfdl.noaa.gov/hiram.

We conducted three HiRAM simulations at C360 grid resolution (approximately 25 km), typically a range that most regional climate models use in climate downscaling studies. This allows us to study regional climate changes using a global climate model that fully accounts for regional- and global-scale interactions, which are especially important in the tropics. A brief description of the methodology and experimental setup is as follows.

We forced HiRAM model simulations with the observed monthly sea surface temperature taken from the Hadley Centre Sea Ice and Sea Surface Temperature data set (Rayner et al., 2003). The sea-ice part of the model assumes that each grid point is either ice free or fully ice covered and also assumes a uniform ice thickness of 2 m. The anthropogenic greenhouse gases, ozone, natural forcings, tropospheric aerosol concentration, and land use changes employed in the model follow the Atmospheric Model Intercomparison Project simulation style (1979- at least 2008; Taylor et al., 2009, 2012), which is described in detail at https://pcmdi.llnl.gov/mips/cmip5/experiment_design.html and http://www.ipcc-data.org/sim/

gcm_monthly/AR5/CMIP5-Experiments.html. The stratospheric volcanic aerosol spatial-time distribution and optical characteristics of volcanic eruptions falling in the simulation period of 1976–2008 (i.e., El Chichon and Pinatubo) are calculated, following Stenchikov et al. (2006) based on Sato et al. (1993). The indirect effect of aerosol particles through microphysical interaction with clouds and associated changes in cloud properties is not considered. Three different realizations were produced, each for a 33-year (1976–2008) simulation period and each beginning with different atmospheric initial conditions, taken from the GFDL long Atmospheric Model Intercomparison Project run at 1 January of years 1976, 1977, and 1978. In all three realizations, the first 3 years of the integration are not used in the analysis, in order to avoid spin-up effects. To reduce the effect of internal natural variability in the model results, ensemble average over three HiRAM realizations is used in the analysis.

For validation of climate trends and the impact of leading circulation modes in the MENA region during the period 1979–2008, we used University of Delaware (UDEL) monthly global gridded temperature and precipitation data (0.5° × 0.5° horizontal grid resolution). The details of UDEL data set can be found at the UDEL website: http://climate.geog.udel.edu/~climate/. A two-tailed student *t* test is applied to find the statistical significance of trends and regression coefficients at a 95% confidence level, both in the model and the observations (see, e.g., Santer et al., 2000 for details).

2.2. Methodology

2.2.1. Multiple Linear Regression Analysis

In this study, we conduct MLR analysis on surface air temperature and precipitation fields using simulated and observed anomalies for 30-year period (1979–2008) and compare the modeled and observed responses of trends and regression coefficients of ENSO, NAO, and ISM over MENA region. We also conduct multiple regression using a 109-year observation period (1900–2008). In the winter season, we perform the MLR analysis by employing a climate trend index (which references to the calendar year of the studied season), the ENSO index (DJF sea surface temperature anomaly in the Niño 3.4 region), and the NAO index (Hurrell, 1995; Hurrell & Deser, 2010), whereas in the summer season we consider the climate trend index, the ENSO index, and the ISM rainfall index (total summer season rainfall computed over the entire Indian region), introduced in Parthasarathy et al. (1994) and Parthasarathy (1995). We analyzed climate trend (linear for the 30-year interval and polynomial for the 109-year interval), ENSO, and NAO in winter season. However, for summer, we considered climate trend, ENSO, and ISM. The selection of input predictors for winter and summer season is discussed in detail in section 2.2.2. The multiple regression methodology employed in this study is explained as follows.

The MLR technique is an extension of the simple linear regression technique that is used when more than one independent factors (also termed as a predictors, regressors, input variables, or controlled variables) affect a dependent variable (also referred as predictand, regressand, criterion variable, response variable, outcome, or measured variable). MLR analysis helps to detect change in dependent variable following the change in independent variables. As predictand or dependent variables we choose $T^i_W(\lambda, \phi)$, winter temperature anomaly; $P^i_W(\lambda, \phi)$, winter precipitation anomaly; $T^i_S(\lambda, \phi)$, summer temperature anomaly; and $P^i_S(\lambda, \phi)$, summer precipitation anomaly, which are functions of longitude λ, latitude ϕ, and the time index *i*, which reflects the year of a season and spans all years in the data set. We choose the following indices as input predictors in the multiple regression analysis (see section 2.2.2 for details regarding selection of relevant predictor variables for MENA region):

- Trend index α^i_{TR}—the standardized year of the season,
- ENSO index α^i_{ENSO}—the standardized DJF NINO3.4-based ENSO index,
- NAO index α^i_{NAO}—the standardized DJF NAO index of Hurrell (1995), and
- ISM index α^i_{ISM}—the standardized JJA ISM rainfall index,

which depend only on the time index *i*. Since all the predictors are standardized, the regression relations take the following forms for winter season,

$$T^i_W(\lambda, \phi) = \alpha^i_{TR} \times T^W_{TR}(\lambda, \phi) + \alpha^i_{ENSO} \times T^W_{ENSO}(\lambda, \phi) + \alpha^i_{NAO} \times T^W_{NAO}(\lambda, \phi), \quad (1)$$

$$P^i_W(\lambda, \phi) = \alpha^i_{TR} \times P^W_{TR}(\lambda, \phi) + \alpha^i_{ENSO} \times P^W_{ENSO}(\lambda, \phi) + \alpha^i_{NAO} \times P^W_{NAO}(\lambda, \phi), \quad (2)$$

and for summer season,

$$T^{i}_{S}(\lambda,\phi) = \alpha^{i}_{TR}\times T^{S}_{TR}(\lambda,\phi) + \alpha^{i}_{ENSO}\times T^{S}_{ENSO}(\lambda,\phi) + \alpha^{i}_{ISM}\times T^{S}_{ISM}(\lambda,\phi), \quad (3)$$

$$P^{i}_{S}(\lambda,\phi) = \alpha^{i}_{TR}\times P^{S}_{TR}(\lambda,\phi) + \alpha^{i}_{ENSO}\times P^{S}_{ENSO}(\lambda,\phi) + \alpha^{i}_{ISM}\times P^{S}_{ISM}(\lambda,\phi), \quad (4)$$

where $T^{W,S}_{TR}$, $P^{W,S}_{TR}$, $T^{W,S}_{ENSO}$, $P^{W,S}_{ENSO}$, T^{W}_{NAO}, P^{W}_{NAO}, T^{S}_{ISM}, and P^{S}_{ISM} are the regression coefficients that for each (λ, ϕ) can be obtained from the following systems of linear equations for winter season,

$$\begin{aligned}
\mathrm{Cov}(\alpha^{i}_{TR}, T^{i}_{W}) &= T^{W}_{TR} + \mathrm{cov}(\alpha^{i}_{TR}, \alpha^{i}_{ENSO})\times T^{W}_{ENSO} + \mathrm{cov}(\alpha^{i}_{TR}, \alpha^{i}_{NAO})\times T^{W}_{NAO},\\
\mathrm{Cov}(\alpha^{i}_{ENSO}, T^{i}_{W}) &= \mathrm{cov}(\alpha^{i}_{TR}, \alpha^{i}_{ENSO})\times T^{W}_{TR} + T^{W}_{ENSO} + \mathrm{cov}(\alpha^{i}_{ENSO}, \alpha^{i}_{NAO})\times T^{W}_{NAO},\\
\mathrm{Cov}(\alpha^{i}_{NAO}, T^{i}_{W}) &= \mathrm{cov}(\alpha^{i}_{TR}, \alpha^{i}_{NAO})\times T^{W}_{TR} + \mathrm{cov}(\alpha^{i}_{NAO}, \alpha^{i}_{ENSO})\times T^{W}_{ENSO} + T^{W}_{NAO},\\
\mathrm{Cov}(\alpha^{i}_{TR}, P^{i}_{W}) &= P^{W}_{TR} + \mathrm{cov}(\alpha^{i}_{TR}, \alpha^{i}_{ENSO})\times P^{W}_{ENSO} + \mathrm{cov}(\alpha^{i}_{TR}, \alpha^{i}_{NAO})\times P^{W}_{NAO},\\
\mathrm{Cov}(\alpha^{i}_{ENSO}, P^{i}_{W}) &= \mathrm{cov}(\alpha^{i}_{TR}, \alpha^{i}_{ENSO})\times P^{W}_{TR} + P^{W}_{ENSO} + \mathrm{cov}(\alpha^{i}_{ENSO}, \alpha^{i}_{NAO})\times P^{W}_{NAO},\\
\mathrm{Cov}(\alpha^{i}_{NAO}, P^{i}_{W}) &= \mathrm{cov}(\alpha^{i}_{TR}, \alpha^{i}_{NAO})\times P^{W}_{TR} + \mathrm{cov}(\alpha^{i}_{NAO}, \alpha^{i}_{ENSO})\times P^{W}_{ENSO} + P^{W}_{NAO},
\end{aligned}$$

and for the summer season we have

$$\begin{aligned}
\mathrm{Cov}(\alpha^{i}_{TR}, T^{i}_{S}) &= T^{S}_{TR} + \mathrm{cov}(\alpha^{i}_{TR}, \alpha^{i}_{ENSO})\times T^{S}_{ENSO} + \mathrm{cov}(\alpha^{i}_{TR}, \alpha^{i}_{ISM})\times T^{S}_{ISM},\\
\mathrm{Cov}(\alpha^{i}_{ENSO}, T^{i}_{S}) &= \mathrm{cov}(\alpha^{i}_{TR}, \alpha^{i}_{ENSO})\times T^{S}_{TR} + T^{S}_{ENSO} + \mathrm{cov}(\alpha^{i}_{ENSO}, \alpha^{i}_{ISM})\times T^{S}_{ISM},\\
\mathrm{Cov}(\alpha^{i}_{NAO}, T^{i}_{S}) &= \mathrm{cov}(\alpha^{i}_{TR}, \alpha^{i}_{NAO})\times T^{S}_{TR} + \mathrm{cov}(\alpha^{i}_{NAO}, \alpha^{i}_{ENSO})\times T^{S}_{ENSO} + T^{S}_{ISM},\\
\mathrm{Cov}(\alpha^{i}_{TR}, P^{i}_{S}) &= P^{S}_{TR} + \mathrm{cov}(\alpha^{i}_{TR}, \alpha^{i}_{ENSO})\times P^{S}_{ENSO} + \mathrm{cov}(\alpha^{i}_{TR}, \alpha^{i}_{ISM})\times P^{S}_{ISM},\\
\mathrm{Cov}(\alpha^{i}_{ENSO}, P^{i}_{S}) &= \mathrm{cov}(\alpha^{i}_{TR}, \alpha^{i}_{ENSO})\times P^{S}_{TR} + P^{S}_{ENSO} + \mathrm{cov}(\alpha^{i}_{ENSO}, \alpha^{i}_{ISM})\times P^{S}_{ISM},\\
\mathrm{Cov}(\alpha^{i}_{NAO}, P^{i}_{S}) &= \mathrm{cov}(\alpha^{i}_{TR}, \alpha^{i}_{NAO})\times P^{S}_{TR} + \mathrm{cov}(\alpha^{i}_{NAO}, \alpha^{i}_{ENSO})\times P^{S}_{ENSO} + P^{S}_{ISM},
\end{aligned}$$

where *Cov* is the covariance operator. For further details see (Gujarati, 2009).

2.2.2. Selection of Leading Predictors Used in MLR for MENA Region

It has been discussed in several studies that the NAO is one of the primary modes of atmospheric variability in the North Atlantic sector that largely impacts the climate of Europe and MENA (Abualnaja et al., 2015; Athar, 2014; Barlow et al., 2016; Hurrell, 1995; Yu & Zhou, 2004). ENSO and ISM (or simply Indian monsoon) have also been reported as important modes of variability that impact MENA climate (Abualnaja et al., 2015; Athar, 2014; Athar & Ammar, 2016; Chakraborty et al., 2006; Wanner et al., 2001). Wanner et al. (2001) and Athar (2014) have shown that both the NAO and ENSO are the prominent modes of variabilities that are essential to be considered while discussing Northern Hemisphere winter climate, especially the climate of AP region. There are other modes of variabilities with origin in the Atlantic sector such as East Atlantic and East Atlantic West Russia (EA/WR) patterns that presumably impact climate of Europe and the Middle East; however, Krichak et al. (2002) have discussed that the impact of EA/WR over Middle East is much less compared to NAO and ENSO impact. They further showed that the precipitation anomalies induced by EA/WR pattern over these regions are not significant. In recent studies, it has been discussed that the EA/WR's pattern impacts Eastern North America and Eurasia including the Ural Mountains, Northeastern Africa, and the Middle East region. However, these studies suggest that this variability pattern is modulated by NAO oscillation, as both are closely associated (Lim, 2015). Wanner et al. (2001) further suggest that the variability in the North Atlantic sector and associated global and regional impacts are largely explained by NAO pattern (which is closely related to Arctic Oscillation) in the North Atlantic Ocean. We also tested the impact of the Indian Ocean Dipole (IOD) on the MENA region and found it small. However, the theory of the IOD itself as an independent mode of variability is still controversial, and the ENSO sea surface temperature teleconnection pattern in the Indian Ocean resembles that of the IOD; therefore, the IOD's independence may not be easy to demonstrate (Kucharski et al., 2010). The Atlantic multidecadal oscillation and Pacific decadal oscillation also seem important control factors on much longer timescales than those considered here. Some studies have focused on the impact of North Sea Caspian teleconnection Pattern (NCP; Kutiel & Benaroch, 2002) over Eastern

Mediterranean with focus over Turkey (Kutiel et al., 2002) and over Iran region (Ghasemi & Khalili, 2008). However, Kutiel et al. (2002) specified that its impact on precipitation is less pronounced compared to its impact on temperature, as the former is influenced by local orography and associated climatic perturbations. The NCP impact in summer season is negligible compared to winter season (Kutiel et al., 2002). Moreover, the regional sensitivity and modulation of this regional-scale NCP mode by large-scale ENSO and NAO circulation modes are not well established hitherto. Hence, to avoid multicolleanearity issue in multiple regression analysis, we did not include NCP index in the present study.

Based on the above discussion, we anticipate that considering NAO and ENSO as leading patterns would be enough to account for most of the variability over MENA region in the winter season. Similarly ENSO and ISM appear to have significant contribution in summer season over MENA (Abualnaja et al., 2015; Almazroui et al., 2012; Athar, 2014; Athar & Ammar, 2016). The ISM plays a significant role in strengthening of the coastal precipitation both in West Africa and over the Horn of Africa to the east by affecting the Intertropical Convergence Zone (ITCZ; i.e., the upward branch of Hadley circulation) and the Somali jet. In the subsequent section we will analyze the NAO, ENSO, and ISM regression coefficients and their climatic relevance for MENA domain.

3. Results and Discussion

3.1. Temperature and Precipitation Linear Trends

Figures 1 and 2 show winter and summer decadal trend, respectively, of MENA temperature/precipitation (top/bottom) fields, which are calculated using MLR analysis using the period 1979–2008. The trend in simulated and observed data set shows a strong spatial and seasonal variability with an overall increase of both the temperature and precipitation, although important disagreements between the UDEL observations and model output are found. The spatial distribution of the winter decadal temperature trend over the entire MENA region (Figure 1) shows that the temperature has an overall growing trend that reaches to 0.5 K per decade both in the UDEL observation and HiRAM output. There exists some spatial inconsistency between observation and model results such that the UDEL observations show maximum warming over central Africa, especially over Sudan, Niger, and Mauritania, whereas the model shows a maximum warming trend over the northeastern part of the selected domain, especially over Iran, Afghanistan, and Turkmenistan. Moreover, observations show a decreasing trend that reaches up to −0.5 K per decade over Turkey, Syria, and Iraq whereas the model does not capture this pattern; instead, it displays an increasing trend distribution over these areas. The decadal trend in winter precipitation shows a mixed pattern with an overall increasing trend over the tropical regions and a decreasing pattern over parts of Southern Europe, AP, and Iran both in the model and observations. The trend distribution of precipitation in winter is largely in agreement (both quantitatively and qualitatively) between the model and UDEL observations, except over Sudan and the Iberian Peninsula, where they show a different spatial structure. The possible difference of the spatial structure and magnitude of the trend between the model and observation could be accounted for by the internal natural climate variability signal, as it needs not to be the same between the model and observation. Large discrepancies in observations and model trends (Figure 1) over the Taurus and Zagros Mountains in temperature, as well as the precipitation, could be partly attributed to the orographic effect that is not well simulated by the HiRAM model (El-Samra et al., 2018). However, further analysis is warranted to quantify the magnitude of the variation caused by the orographic effect and the internal climate variability signal.

Alike its winter counterpart, the long-term trend of temperature in summer is also rising over the entire MENA region except in the tropical areas, where we observe a decreasing tendency both in the model and the observations (Figure 2). That could be counted for by the increased water vapor and cloud distributions caused by the increased land-sea thermal gradient in summer season, which attenuates downward solar radiation resulting in surface cooling. Moreover, the decadal trend of temperature in summer over the northern half of the selected domain is larger, which peaks at 1 K per decade compared to the southern part of the domain that peaks at 0.5 K per decade, predominantly in the observations. The summer precipitation shows an overall increasing trend, especially over the tropical belt. Moreover, the precipitation shows a dipole structure, with a rising trend (which peaks at 0.5 mm/day per decade both in the model and observations) over the northern areas of the tropics and a decreasing trend southward of 10°N, especially in the UDEL observations. The trend pattern of temperature and precipitation in summer season is relatively more

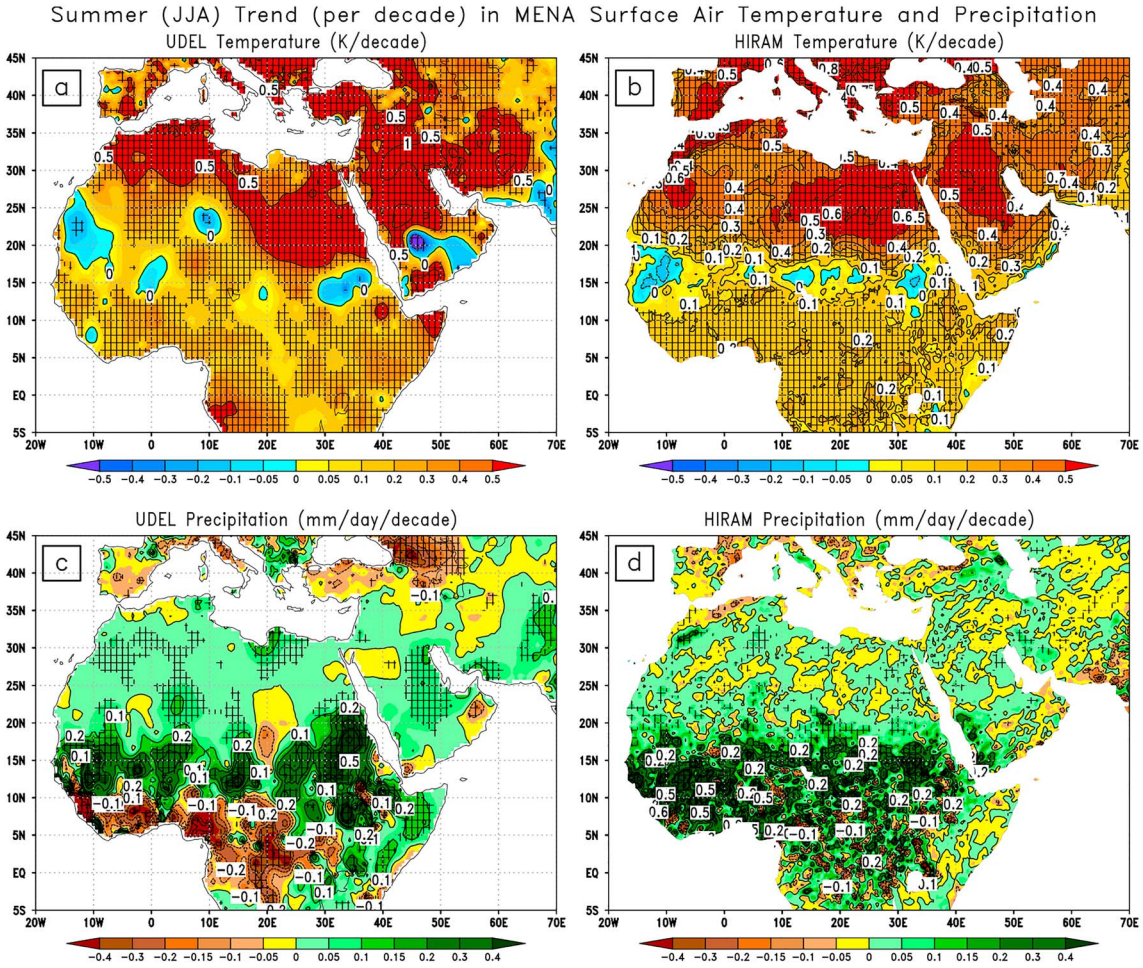

Figure 1. The spatial distributions of the trends (per decade) of winter (DJF) temperature over the period of 1979–2008 using (a) UDEL and (b) HiRAM output and trend in precipitation using (c) UDEL and (d) HiRAM output. Hatching indicates statistically significant decadal trends at 95% confidence level. DJF = December to February; HiRAM = high-resolution atmospheric model; MENA = Middle East and North Africa; UDEL = University of Delaware.

consistent between the model and observation compared to the winter counterpart, suggesting that model performs reasonably well in summer. The long-term trend in data could be associated with the internal noise and large-scale circulation changes such as NAO. It has been noticed in previous studies that the HiRAM model, like other up-to-date climate models, underestimates the response of NAO in winter (Dogar, Stenchikov, et al., 2017; Driscoll et al., 2012). The presented trend maps, both for winter and summer seasons, show that the climate trends could add uncertainty in the forcings-induced climate signals and therefore need to be filtered out while examining temperature and precipitation changes caused by internal and external climate forcing factors such as volcanism, NAO, and ENSO. The presented long-term decadal trend results are consistent with earlier studies (e.g., Athar, 2014; Krishna, 2014), which also show an overall increasing temperature trend. We further find that the values of the decadal trend of temperature, especially in the northern part of the selected domain, are relatively larger in summer than in winter. Moreover, the decadal trend of temperatures in both the seasons has statistically significant and relatively larger trend values, which are spatially more widespread compared to the precipitation decadal trend values.

3.2. Temperature and Precipitation Polynomial Trends

To see the robustness of temperature and precipitation trends and to further understand the long-term climatic changes over MENA region, we extended the trend analysis over a longer period 1900–2008 and computed trends in the temperature and precipitation fields using UDEL observed data set. For this purpose we computed polynomial trends, as the trends over longer period are not linear (Dogar, Stenchikov, et al.,

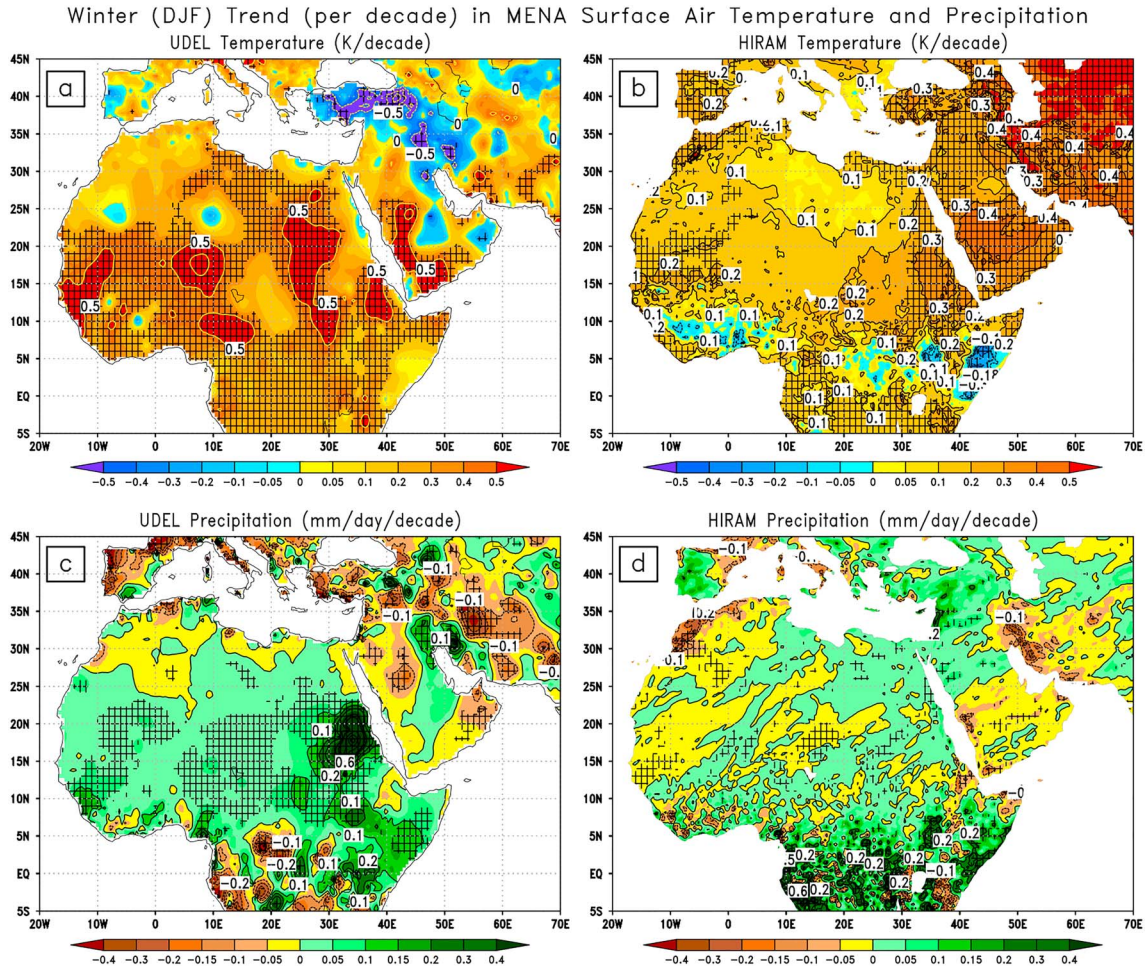

Figure 2. The spatial distributions of the trends (per decade) of summer (JJA) temperature over the period of 1979–2008 using (a) UDEL and (b) HiRAM output and trend in precipitation using (c) UDEL and (d) HiRAM output. Hatching indicates statistically significant decadal trends at 95% confidence level. DJF = December to February; HiRAM = high-resolution atmospheric model; MENA = Middle East and North Africa; UDEL = University of Delaware.

2017). Figure 3 shows polynomial trend curve computed by averaging over the entire MENA region for both the seasons. The polynomial trend over the longer period reveals that the MENA temperature has an overall increasing trend whereas precipitation has a decreasing trend. However, the long-term temporal evolution of temperature trend both in the winter and summer seasons shows an increasing trend curve for initial few decades, and then it decreases for the period of 1920–1970. The decrease in temperature trend is more obvious in summer season than in winter. After year 1970 the temperature trend increases again. The polynomial trend of precipitation over MENA region has a downtrend for the entire period of analysis in both the seasons such that the decrease is slow in the initial decades and then it becomes relatively more pronounced especially after the year 1920. This analysis of trend using polynomial approach suggests that one has to consider removing polynomial trend from the data while considering analysis over longer period of time, which is 1900–2008 in our case. The temperature and precipitation anomaly for both the seasons before (red curve) and after (green curve) removing polynomial trend is also shown in Figure 3, indicating that the trends add significant part in the anomaly signal and therefore need to be filtered out while considering climatic impact assessment for the MENA region.

3.3. NAO, ENSO, and ISM Regression Coefficients

Using MLR analysis (see section 2 for details), we computed regression coefficients of ENSO, NAO, and ISM, which explain their long-term seasonal summer and winter climatic impact on MENA temperature and precipitation fields. The regression coefficient maps are helpful to summarize our understanding of consistent NAO, ENSO, and Indian monsoon relations with MENA surface temperature and precipitation fields. As

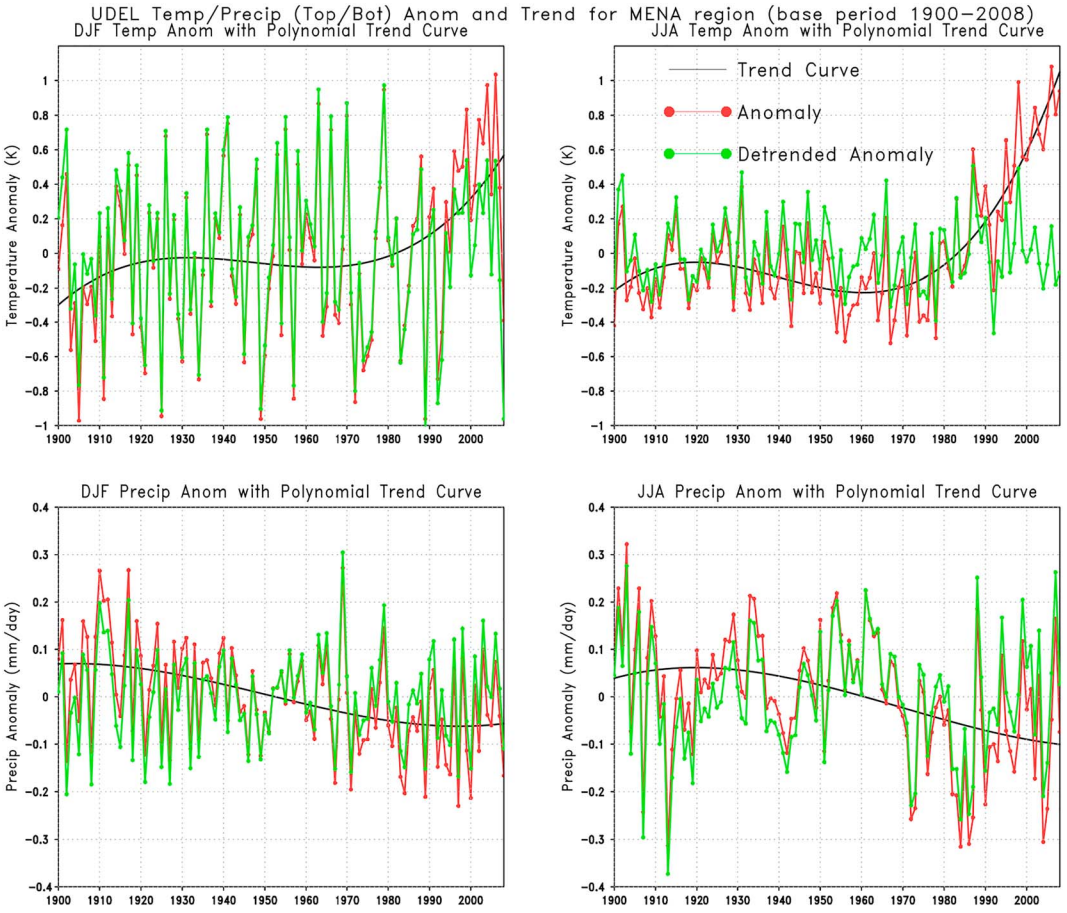

Figure 3. The polynomial trend curve of temperature/precipitation (top/bottom) fields in winter/summer (left/right) computed for MENA region over a longer period of 1900–2008. The anomalies of temperature and precipitation before (red curve) and after removing polynomial trend (green curve) are also shown. DJF = December to February; JJA = June to August; MENA = Middle East and North Africa; UDEL = University of Delaware.

discussed above, the selection of the predictors used in multiple regression analysis are based on their strong correlation with MENA climate as well as their significant climatic impact discussed in the previous literature (see section 2.2.2 for details regarding the selection of independent input variables for MENA region in the winter and summer seasons). These regression coefficients represent the mean change in the dependent variable (temperature or precipitation) for one unit change in the corresponding predictor variable while holding the other predictors to be constant. In the following sections we will discuss each factor in detail.

3.3.1. NAO

The NAO plays a significant role to characterize the atmosphere of Europe and Middle East region (Cullen et al., 2002; Hurrell, 1995; Iqbal et al., 2013; van Loon & Rogers, 1978; Wallace & Gutzler, 1981). Figure 4 displays NAO correlation coefficient with surface air temperature of Eurasia and MENA in winter and summer seasons computed using UDEL observation and HiRAM model over a period of 1979–2008. Both the model and observation depict highly significant positive correlation in winter over northern part of Eurasia, suggesting that the positive NAO phase significantly warms the northern part of Europe and Asia. Similarly, we observed that NAO is negatively correlated with winter temperature of Southern Europe and MENA and its cooling impact further extends to South and East Asia. Spatial structure of NAO correlation with winter temperature of Europe and MENA region shows a dipole nature with positive correlation over Northern Europe and Siberia and negative correlation over midlatitude MENA domain. This suggests that the positive phase of NAO brings cooler and drier air into the Southern Europe and Middle East region, whereas negative phase brings warm and wet conditions over this region. The spatial patterns of temperature and precipitation fields clearly reveal that positive NAO will induce a cooling and drying pattern in winter. These results are consistent with earlier studies (Dogar, Stenchikov et al., 2017; Yu & Zhou, 2004), which also show strong cooling and

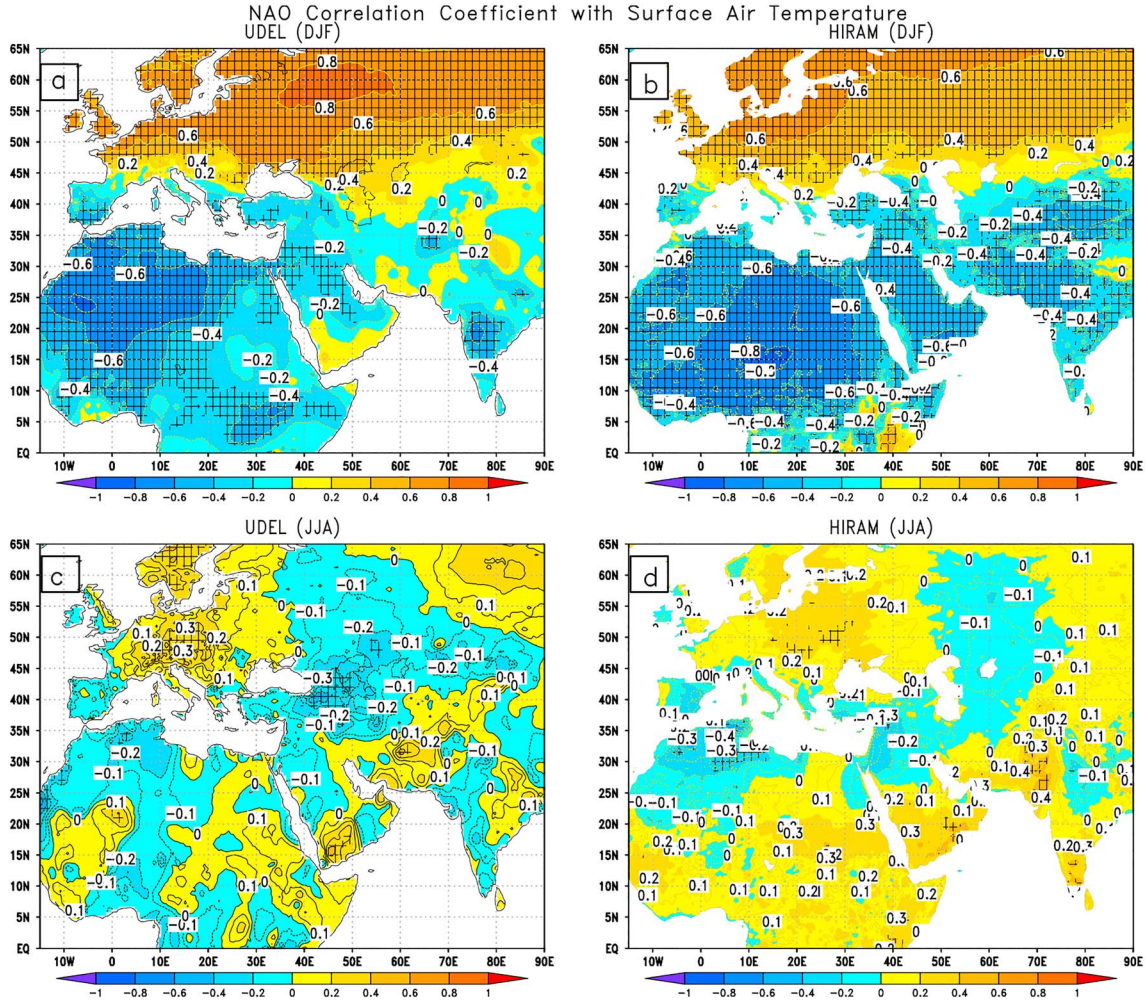

Figure 4. Winter (DJF) NAO correlation coefficient with surface air-temperature calculated using (a) UDEL 30-year winter period, (b) model 30-year winter period, (c) UDEL 30-year summer period, and (d) model 30-year summer period. Hatching shows the statistically significant areas with at least 95% confidence level. DJF = December to February; HiRAM = high-resolution atmospheric model; JJA = June to August; MENA = Middle East and North Africa; NAO = North Atlantic Oscillation; UDEL = University of Delaware.

drying over MENA, following positive NAO phase. Temperature response to NAO circulation in winter is anticipated to be larger and more pronounced than in summer season because NAO correlation in winter with MENA temperature is much higher (Figure 4) than corresponding correlation in summer (Bladé et al., 2012; Hurrell et al., 2003; Iles & Hegerl, 2017). The absolute magnitude of NAO correlation coefficient in winter peaks at 0.6 and 0.8, respectively, in the model and observations (Figure 4). These values are statistically significant at 95% confidence level, suggesting that the NAO circulation plays a significant role to characterize climatic changes over MENA region in winter. HiRAM simulation slightly underestimates the magnitude of NAO correlation coefficient in winter season although overall spatial distribution is well captured by the model.

To further understand how the change in NAO influences the MENA region, we looked at the NAO regression coefficient with MENA surface air temperature and precipitation. Figure 5 shows the map of regression coefficient of NAO in winter season computed using multiple regression analysis, which explains the fractions of the variance of temperature and precipitation caused by NAO over MENA region. A detailed methodology dealing with the selection of these input explanatory variables, along with their importance for MENA region, has been discussed in section 2.2.2.

The positive phase of NAO causes strong cooling (that peaks at -0.6 K in UDEL and -0.4 K in the model response) in winter especially over the AP region (Figure 5), which is consistent with earlier studies that

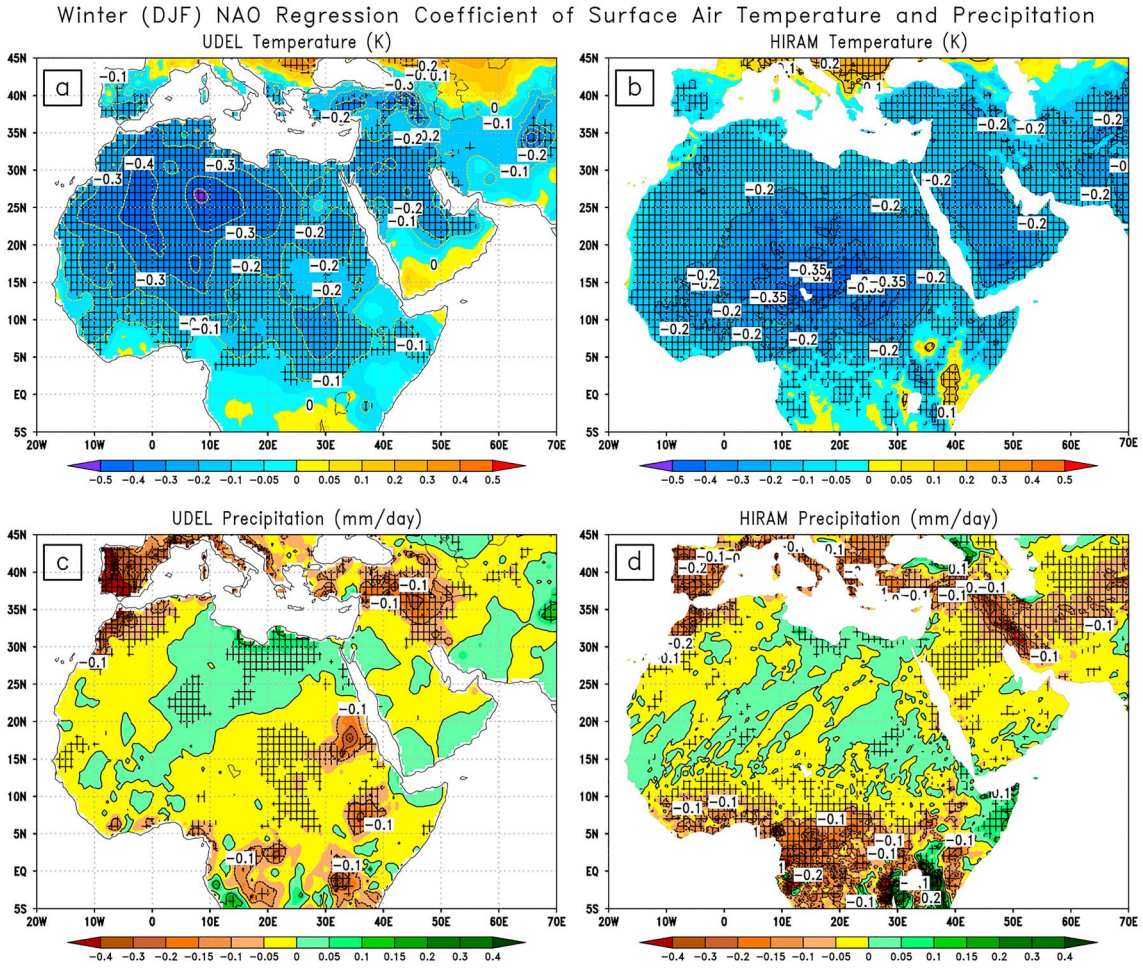

Figure 5. Winter (DJF) NAO regression coefficient with surface air-temperature (K) calculated using (a) UDEL 30-year period and (b) model 30-year period and with precipitation (mm/day) calculated using (c) UDEL 30-year period and (d) model 30-year period. Hatching shows the statistically significant areas with at least 95% confidence level. DJF = December to February; HiRAM = high-resolution atmospheric model; NAO = North Atlantic Oscillation; UDEL = University of Delaware.

used simple linear regression (see, e.g., Iles & Hegerl, 2017; Yu & Zhou, 2004). Moreover, the positive NAO phase results in weakening of rainfall over the entire MENA region, mainly over Southern Europe extending to Iraq and Iran. The NAO-induced patterns are largely consistent between the model and observation. The patterns of NAO regression coefficients, both for UDEL observation and HiRAM output, represent statistically significant response over the entire MENA region. Moreover, it is observed that the NAO-based temperature and precipitation changes in summer season over the MENA are weaker. These results are consistent with earlier studies (Bladé et al., 2012; Hurrell et al., 2003; Iles & Hegerl, 2017). It is expected because the NAO correlation with MENA temperature in summer season is weaker (Figure 4, lower panel).

3.3.2. ENSO

The ENSO atmospheric teleconnections is considered as the leading mode of variability that causes profound effect on global and regional climate and weather events (Azharuddin & Dogar, 2016; Dogar et al., 2018; Kumar et al., 2016; Neelin et al., 1998; Timmermann et al., 1999; Trenberth et al., 1998; Trenberth & Caron, 2000). It has been shown that the climate of Middle East, in particular the AP region, is strongly impacted by ENSO (Abid et al., 2018; Athar & Ammar, 2016; Barlow et al., 2016; Dogar, Kucharski, et al., 2017; Dogar, Stenchikov, et al., 2017; Sandeep & Ajayamohan, 2018). In this section we emphasized that both the El Niño and La Niña are important modes of variability that should be taken into account while discussing leading climate forcing factors and their climatic impacts in the MENA region. By modulating the near-equatorial zonal atmospheric overturning circulation, that is, the Walker circulation, ENSO atmospheric teleconnections induce changes in cloud cover and evaporation in remote ocean basins such as the Arabian Sea, Indian Ocean, and the tropical North Atlantic Ocean that in turn affects the land regions of Middle East and Asia

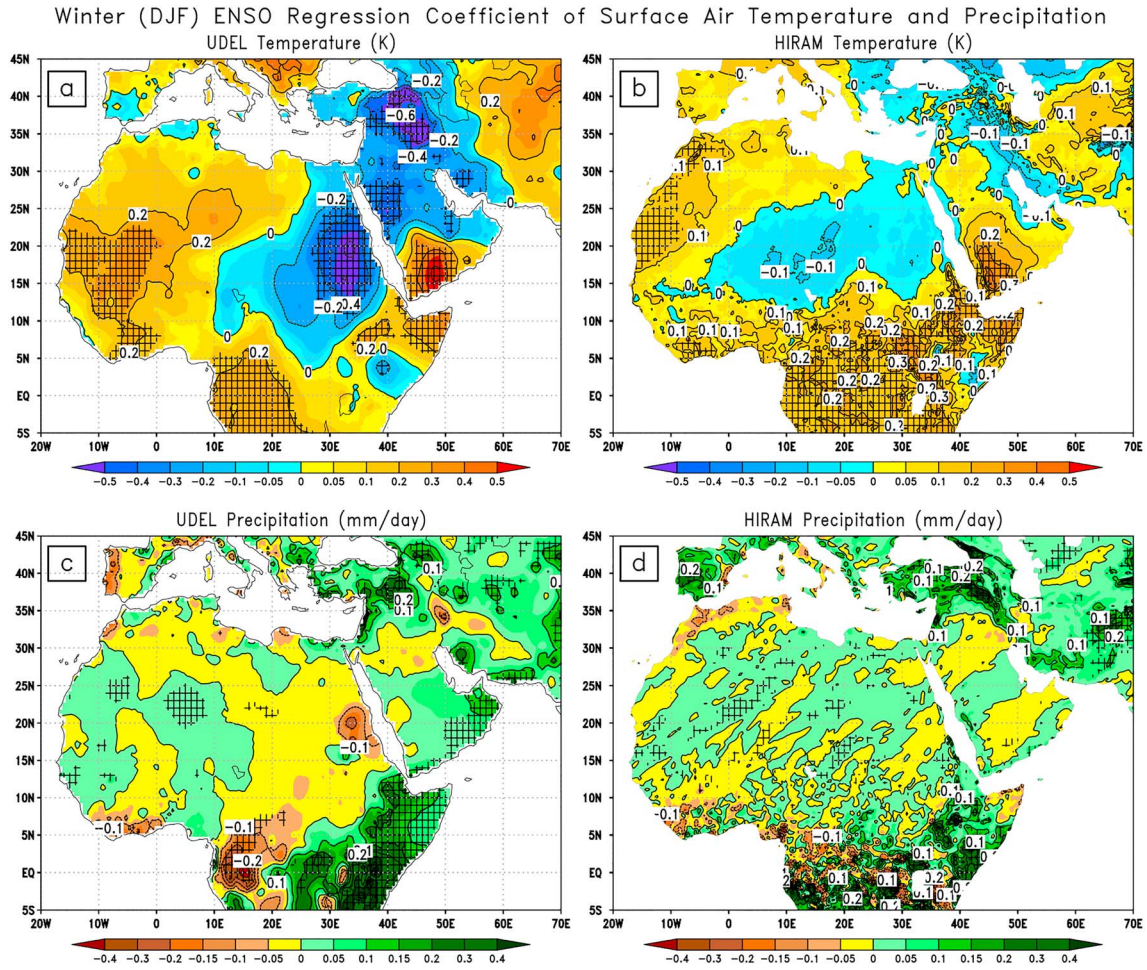

Figure 6. Winter (DJF) ENSO regression coefficient with surface air-temperature (K) calculated using (a) UDEL 30-year period and (b) model 30-year period and with precipitation (mm/day) calculated using (c) UDEL 30-year period and (d) model 30-year period. Hatching shows the statistically significant areas with at least 95% confidence level. DJF = December to February; ENSO = El Niño Southern Oscillation; HiRAM = high-resolution atmospheric model; UDEL = University of Delaware.

(Barlow et al., 2016; Klein et al., 1999; Wang, 2002). For example, during a developing period of El Niño, the Walker circulation moves to the east, resulting in anomalous atmospheric subsidence over the Indian Ocean region and consequent suppression of convection there. This ENSO-induced changes lead to warming in the Indian Ocean through intensified solar radiation as well as a weakening land-sea contrast in summer, resulting in less ISM rainfall. Moreover, ENSO (El Niño/La Niña) is reported to produce increased/decreased precipitation activity over tropical MENA region by inducing thermal changes in the Indian and Atlantic Ocean in winter season, and the reverse is observed for the summer season. To see long-term ENSO effects over the MENA region, we have analyzed their regression coefficients using multiple regression analysis.

Figure 6 shows the map of regression coefficients of ENSO in the winter season, computed using multiple regression analysis, which explains the fractions of the variance of temperature and precipitation caused by ENSO over MENA region. A detailed methodology dealing with the selection of these input explanatory variables, along with their importance for MENA region, has been discussed in section 2.2.2.

The warming phase of ENSO, that is, El Niño, results in cooling over AP and warming over Northwestern as well as tropical parts of Africa (Figure 6). Moreover, the El Niño phase shows increased precipitation over the horn of Africa as well as over North Eastern part, in particular over Iraq and Iran domain. The model shows slightly weaker regression coefficient values than the observations, and the spatial patterns are also somewhat shifted in the model compared to observation. The ENSO (El Niño/La Niña) regression coefficients show that the temperature change (cooling/warming) caused by ENSO reaches a maximum absolute value of 0.6/0.4 K in the observation and 0.1/0.3 K in the model. However, these cooling/warming impacts are

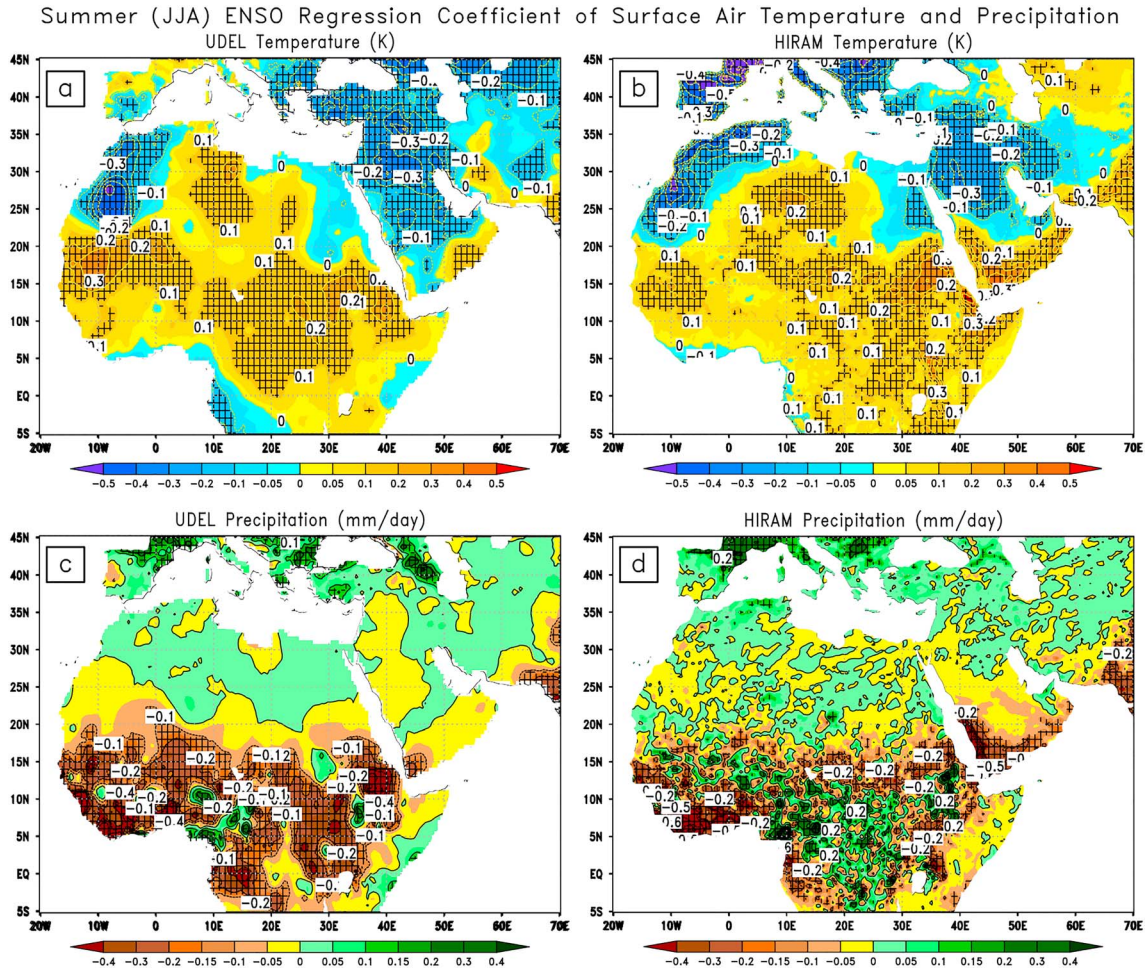

Figure 7. Summer (JJA) ENSO regression coefficient with surface air-temperature (K) calculated using (a) UDEL 30-year period and (b) model 30-year period and with precipitation (mm/day) calculated using (c) UDEL 30-year period and (d) model 30-year period. Hatching shows the statistically significant areas with at least 95% confidence level. ENSO = El Niño Southern Oscillation; HiRAM = high-resolution atmospheric model; JJA = June to August; UDEL = University of Delaware.

statistically significant especially in the observations, suggesting that ENSO produces substantial climatic signal over MENA region in the winter season.

The MENA region is also strongly influenced by ENSO in summer season as explained by the ENSO regression coefficients for temperature and precipitation (Figure 7). The ENSO (El Niño/La Niña) results in significant (at 95% confidence level) warming/cooling and decreased/increased precipitation over the tropical rain belt regions of MENA in summer both in the model and observations. The ENSO-induced warming/cooling and drying/wetting over MENA ranges absolute value between 0.1 to 0.5 K for temperature and 0.1 to 0.6 mm/day for precipitation as seen from the summer ENSO regression coefficients (Figure 7) computed using MLR over the period of 1979–2008. The El Niño induced summer warming and drying over MENA tropical region peaks at 0.3 K and -0.6 mm/day respectively. From the spatial pattern of temperature and precipitation, we observed that the temperature- and pressure-based indices, that is, ENSO and NAO, respectively, have a higher value of statistically significant regression coefficients and are spatially more widespread as compared to the precipitation-based indices, that is, ISM (section 3.3.3).

3.3.3. ISM

Several studies have emphasized that the global monsoon systems, especially the Indian and African monsoons, are strongly affected by the internal and external climate forcing factors (Anchukaitis et al., 2010; Joseph & Zeng, 2011; Liu et al., 2016; Oman et al., 2006; Trenberth & Dai, 2007). It has also been observed that the temperature and rainfall distribution of the MENA tropical region in summer is largely characterized by the strength of its monsoon system (Rodwell & Hoskins, 1996; Sultan & Janicot, 2000). External

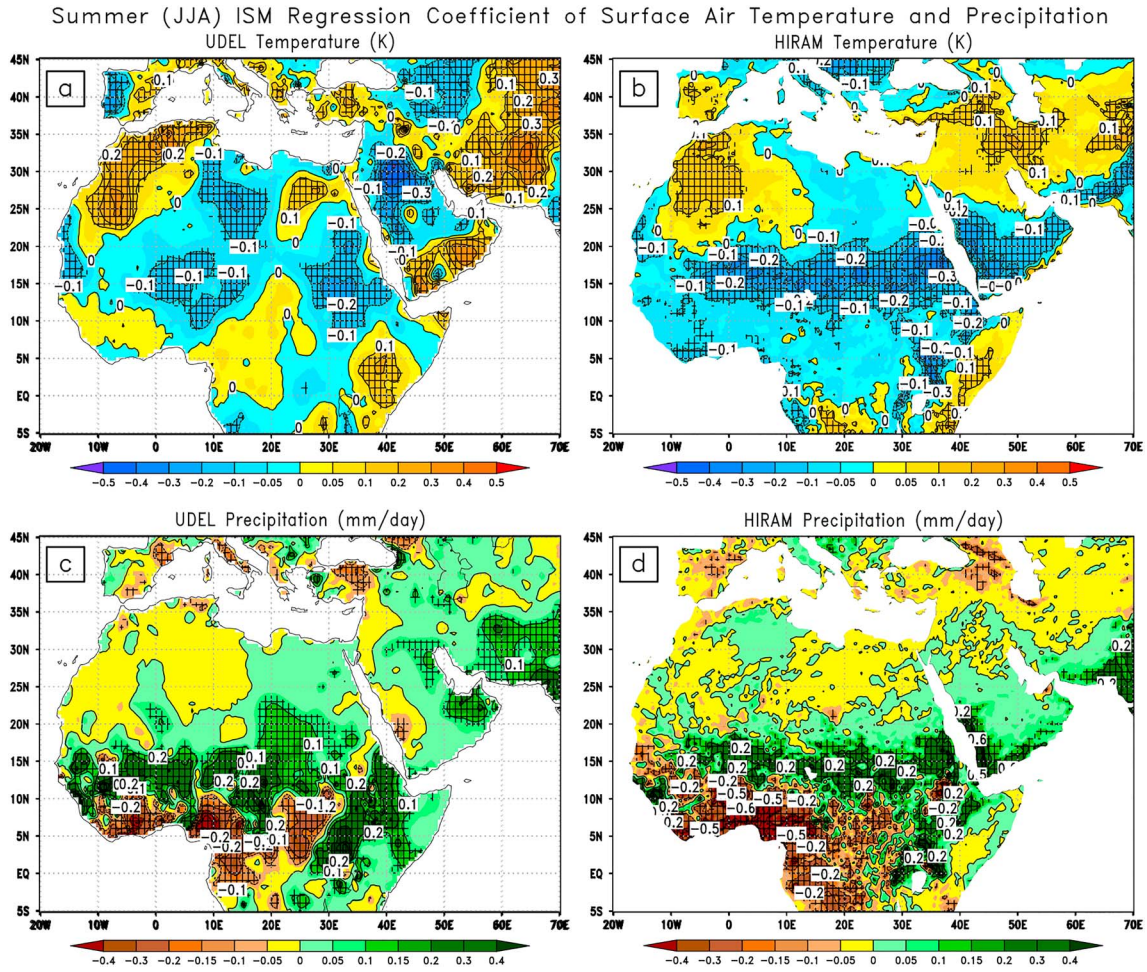

Figure 8. Summer (JJA) ISM regression coefficient of surface air-temperature (K) calculated using (a) UDEL 30-year period and (b) model 30-year period and with precipitation (mm/day) calculated using (c) UDEL 30-year period and (d) model 30-year period. Hatching shows the statistically significant areas with at least 95% confidence level. HiRAM = high-resolution atmospheric model; ISM = Indian summer monsoon; JJA = June to August; UDEL = University of Delaware.

forcings such as explosive eruptions induce weakening to the monsoon system (Liu et al., 2016; Oman et al., 2006) and affect the position of ITCZ (Dogar, Stenchikov, et al., 2017; Haywood et al., 2013). Earlier studies have shown that Indian and African monsoon systems are tightly linked to the rising branch of local Hadley cell, also known as ITCZ (Joseph & Zeng, 2011; Wegmann et al., 2014). Hence, the Indian and African monsoons are affected by climate forcings-induced seasonal changes in the ITCZ (Wegmann et al., 2014). In summer season, ITCZ moves northward as a result of climate forcings-induced thermal gradient between land and ocean. This interhemispheric gradient drives Hadley circulation. A decreased land-sea thermal gradient following external or internal forcings suppresses the northward migration of ITCZ that results into a decreased amount of clouds and associated decrease in rainfall over the tropical ITCZ region. Moreover, the tropical climate of the AP and East Africa region is largely affected by the intensity of the Somali jets that are driven by the strength of the Indian monsoon system. A stronger Indian monsoon system drags immense moisture (through Somali jet) toward inland region of East Africa (Uganda, South Sudan, Kenya, Somalia, Ethiopia, Djibouti, and Eritrea) and southern parts of AP including Yemen and Oman. This moist wind system (Somali jet) then, following geostrophic wind relation, enters to northern and central India because of strong low pressure system over Indian landmass during summer period, whereas a weakened Indian monsoon will have weakened Somali current that will result in less transport of moisture laden air to Central and Eastern Africa (Aiki et al., 2006) and to the north and central India that consequently affects Hadley rising branch.

A strong teleconnection effect of Indian monsoon on African monsoon system, especially the influence of Indian monsoon on East and West African monsoon onset, is shown in previous studies (Camberlin et al., 2010; Flaounas et al., 2012). Based on regression analysis, we also observed that Indian and African monsoon systems are well correlated and therefore a weakened Indian and African monsoon will produce warming and drying anomaly over tropical MENA region.

As discussed above, the MENA region is strongly influenced by the Indian monsoon in summer season as explained by the ISM regression coefficient for temperature and precipitation (Figure 8). An increased ISM results in decreased/increased (temperature/precipitation) over the tropical parts of the MENA region in summer. The absolute value of ISM regression coefficients for temperature/precipitation fields peaks at 0.4/0.6, and these values are statistically significant, especially over the tropical areas, suggesting that ISM produces significant climatic impact over MENA tropical regions in summer. Both the model and observations show significant warming over Iran, Afghanistan, and northwestern African domain, especially over Morocco that extends to southern Europe, suggesting that ISM produces wide-ranging climatic impacts. The spatial pattern of ISM regression coefficient, especially for temperature case, is relatively less smooth in the observations, compared to the model, probably because the observational data face scarcity in observational measurements for this region. However, model shows much smoother response (both for temperature and precipitation) presumably because model results are averaged over three ensemble members that possibly minimize the effect of internal noise. The conducted multiple regression analysis emphasizes that the Indian monsoon modulates the strength of African monsoon and therefore a decreased Indian monsoon will produce a decreased precipitation over tropical MENA region. Indian monsoon-induced precipitation distribution shows a dipole structure at Northern Hemisphere tropical region (decreased precipitation northward of 10°N and subsequent increase southward of 10°N), which could be attributed to the southward shift of ITCZ (Dogar, Stenchikov, et al., 2017; Haywood et al., 2013; Liu et al., 2016). This pattern suggests that a significant portion of the total precipitation over MENA tropical region is controlled by the strength of Indian monsoon as it could cause weakening to the rising branch of NH local Hadley circulation, that is, the ITCZ. A detailed discussion on possible mechanisms and teleconnection between Asian monsoon system and precipitation changes over MENA (through monsoon-desert mechanism) can be seen in Rodwell and Hoskins (1996). Our results are largely consistent with earlier studies that deal with ENSO and Indian monsoon changes over African region using modeling and observational approaches (Preethi et al., 2015).

From the spatial pattern of temperature and precipitation, we observed that the temperature- and pressure-based indices, that is, ENSO and NAO, respectively, have a higher value of statistically significant regression coefficients and are spatially more widespread compared to the precipitation-based indices, that is, ISM.

4. Summary and Conclusions

Both the climate trends and the regression coefficients of leading climate variability modes are important parameters that are widely used to study the global and regional climatic changes induced by internal and external climate forcings. This paper focuses on the importance of trend in data and leading climate variability modes that play significant role in shaping MENA climate in winter and summer seasons. As MENA region is very sensitive to the changes induced by the internal and external climate forcings, thereby, understanding the processes that govern MENA climatic variability is of high priority, especially in the context of global and regional climate change. In order to better understand the climatic impact of leading modes of variabilities (i.e., their spatial structure, temporal evolution, mechanism, and climate variability) over MENA region, we used multiple regression analysis and looked at the impact of leading variability modes over the MENA temperature and precipitation fields. Regression analysis is widely used to identify the spatial patterns of climate change that are associated to internal and forced climate variability. The selection of leading predictors used in multiple regression analysis for MENA region is based on their importance highlighted in the literature as well as our own assessment based on their strong correlation with MENA temperature and precipitation fields. For the analysis of trend in data we computed linear and polynomial trends over the periods 1979–2008 and 1900–2008, respectively. We used polynomial trend for the longer 109-year period (1900–2008), as the trends over longer period are not linear. For better comparison of associated climatic impact, the trend and other leading predictors are standardized. The conducted MLR analysis emphasizes that the trend in data could add significant contribution (it may add uncertainty or noise in climate signal) in climate variability pattern of a region

and therefore trend-induced contribution needs to be filtered out while analyzing the impact of different leading factors. Our results further emphasize that NAO, ENSO, and ISM are the leading variability modes that significantly impact the climate of MENA. The positive phase of NAO causes cold and dry climatic changes over the MENA region in winter. The impact of NAO in summer is much weaker than its winter counterpart. It is expected because the NAO correlation with MENA temperature in summer is weaker and less significant than its winter counterpart. ENSO (El Niño/La Niña) also induces cold/warm anomalies over the AP in winter season. Moreover, ENSO (El Niño/La Niña) brings warm/cold and associated dry/wet climatic changes especially over the MENA tropical region in summer season through ENSO-induced thermal changes in the Indian and Atlantic Ocean that in turn affect MENA tropical land areas. Indian monsoon also plays significant role to characterize the climate of MENA and South Asia in the summer season. A weaker Indian monsoon will cause weakening to Hadley circulation and weakening to the Somali current that in turn affect the cloud distribution and moisture entrainment toward inland regions of south Asia and MENA. The analysis of trends and regression coefficients is necessary to better understand the climate variability of MENA. Both the observational and simulated results highlight the need to better understand the long-term trend in data and to better account for the circulation responses, such as that of the NAO, ENSO, and ISM to better understand the MENA regional climate variability.

In this research, we used a high-resolution global climate model, at a very high resolution, typically used by regional climate models in climate downscaling studies, which is especially important to better simulate the regional impacts of global teleconnection patterns. The main findings and results of this study can be summarized as follows.

MENA shows a significant upward temperature trend that reaches to 0.5 and 1 K per decade during the winter and summer period, respectively, both in the observations and model response. The precipitation shows a mixed trend pattern in winter; however, in summer, a decreased precipitation especially over the tropical belt, reaching to 0.5 mm/day per decade, is observed. The polynomial trend produced by averaging over entire MENA domain, considered for the longer period (1900–2008), depicts downward temperature trend line during 1900–1920, constant during 1920–1970 and strong upward temperature trend during the period 1970–2008, both in winter and summer seasons, suggesting that one has to consider polynomial trend while discussing climatic impacts of trends and leading teleconnections over longer period.

Both the ENSO and NAO positive phases significantly cool the central parts of MENA in winter over the period 1979–2008, especially the AP region. The positive phase of NAO produces strong cooling in winter over the entire MENA that reaches to -0.6 and -0.4 K in the observation and model, respectively. The model underestimates the winter cooling response (both for ENSO and NAO); however, the overall pattern is well reproduced by the model. The impact of NAO in summer is small, as the correlation of NAO in summer is much weaker than its winter counterpart. The warm ENSO phase in summer produces strong tropical warming and drying that peaks at 0.3 K and -0.6 mm/day respectively both in the model and observations. Our results further reveal that the Indian monsoon also produces strong impact over the MENA region, by impacting the MENA ITCZ and associated cloud distribution. A strengthening (weakening) of ISM results in strengthening (weakening) and associated increased (decreased) cloud distribution over MENA tropical rain belt region, resulting in increased (decreased) precipitation. A strengthening/weakening of ISM produces substantial temperature and precipitation changes over MENA, resulting in cooling/warming (wetting/drying) over MENA tropical rain belt regions that peaks at 0.4 K/0.6 mm/day (absolute value), suggesting that ISM produces significant climatic impact over MENA tropics in summer. A decreased ISM suggests a southward shift of ITCZ. The possible difference of the spatial structure and magnitude of the trend between the model and observation could be accounted for by the internal natural climate variability signal, as it needs not to be the same between the model and observation. The disagreements in observations and model results over the Taurus and Zagros Mountains in temperature and precipitation trends over MENA in winter season are attributed to the orographic effect that is not well simulated by the HiRAM model. The conducted analysis sheds light on the internal mechanisms of MENA climate variability and helps to selectively diagnose the impact of leading teleconnection modes.

Acknowledgments
The King Abdullah University of Science and Technology (KAUST), Thuwal, Saudi Arabia, supported the research reported in this publication. The GFDL-HiRAM simulation data can be accessed from http://nomads.gfdl.noaa.gov:8080/DataPortal/cmip5.jsp. The UDEL observation data set used in this study is provided by the NOAA/OAR/ESRL PSD, Boulder, Colorado, United States, through their web site at http://www.esrl.noaa.gov/psd/.

References

Abid, M. A., Almazroui, M., Kucharski, F., O'Brien, E., & Yousef, A. E. (2018). ENSO relationship to summer rainfall variability and its potential predictability over Arabian Peninsula region. npj. *Climate and Atmospheric Science*, *1*(1), 1.

Abualnaja, Y., Papadopoulos, V. P., Josey, S. A., Hoteit, I., Kontoyiannis, H., & Raitsos, D. E. (2015). Impacts of climate modes on air-sea heat exchange in the Red Sea. *Journal of Climate*, *28*(7), 2665–2681. https://doi.org/10.1175/JCLI-D-14-00379.1

Aiki, H., Takahashi, K., & Yamagata, T. (2006). The Red Sea outflow regulated by the Indian monsoon. *Continental Shelf Research*, *26*(12-13), 1448–1468. https://doi.org/10.1016/j.csr.2006.02.017

Almazroui, M., Islam, N. M., Athar, H., Jones, P. D., & Rahman, M. A. (2012). Recent climate change in the Arabian Peninsula: Annual rainfall and temperature analysis of Saudi Arabia for 1978–2009. *International Journal of Climatology*, *32*(6), 953–966. https://doi.org/10.1002/joc.3446

AlSarmi, S., & Washington, R. (2011). Recent observed climate change over the Arabian Peninsula. *Journal of Geophysical Research*, *116*, D11109. https://doi.org/10.1029/2010JD015459

AlSarmi, S. H., & Washington, R. (2013). Changes in climate extremes in the Arabian Peninsula: Analysis of daily data. *International Journal of Climatology*, *34*(5), 1329–1345. https://doi.org/10.1002/joc.3772

Anchukaitis, K., Buckley, B., Cook, E., Cook, B., D'Arrigo, R., & Ammann, C. (2010). Influence of volcanic eruptions on the climate of the Asian monsoon region. *Geophysical Research Letters*, *37*, L22703. https://doi.org/10.1029/2010GL044843

Anderson, J. L., Balaji, V., Broccoli, A. J., & Cooke, W. F. (2004). The new GFDL global atmosphere and land model AM2-LM2: Evaluation with prescribed SST simulations. *Journal of Climate*, *17*(24), 4641.

Athar, H. (2014). Trends in observed extreme climate indices in Saudi Arabia during 1979–2008. *International Journal of Climatology*, *34*(5), 1561–1574. https://doi.org/10.1002/joc.3783

Athar, H., & Ammar, K. (2016). Seasonal characteristics of the large-scale moisture flux transport over the Arabian Peninsula. *Theoretical and Applied Climatology*, *124*(3-4), 565–578. https://doi.org/10.1007/s00704-015-1437-7

Azharuddin, S., & Dogar, M. M. (2016). Decadal climate variability and predictability. *Current Science*, *110*(8), 1397–1398.

Bangalath, H., & Stenchikov, G. (2015). Role of dust direct radiative effect on the tropical rain belt over Middle East and North Africa: A high-resolution AGCM study. *Journal of Geophysical Research: Atmospheres*, *120*, 4564–4584. https://doi.org/10.1002/2015JD023122

Barlow, M., Zaitchik, B., Paz, S., Black, E., Evans, J., & Hoell, A. (2016). A review of drought in the Middle East and Southwest Asia. *Journal of Climate*, *29*(23), 8547–8574. https://doi.org/10.1175/jcli-d-13-00692.1

Bladé, I., Liebmann, B., Fortuny, D., & van Oldenborgh, G. J. (2012). Observed and simulated impacts of the summer NAO in Europe: Implications for projected drying in the Mediterranean region. *Climate Dynamics*, *39*(3–4), 709–727. https://doi.org/10.1007/s00382-011-1195-x

Bretherton, C. S., McCaa, J. R., & Grenier, H. (2004). A new parameterization for shallow cumulus convection and its application to marine subtropical cloud-topped boundary layers. Part I: Description and 1D results. *Monthly Weather Review*, *132*(4), 864–882. https://doi.org/10.1175/1520-0493(2004)132<0864:ANPFSC>2.0.CO;2

Camberlin, P., Fontaine, B., Louvet, S., Oettli, P., & Valimba, P. (2010). Climate adjustments over Africa accompanying the Indian monsoon onset. *Journal of Climate*, *23*(8), 2047–2064. https://doi.org/10.1175/2009JCLI3302.1

Chakraborty, A., Behera, S. K., Mujumdar, M., Ohba, R., & Yamagata, T. (2006). Diagnosis of tropospheric moisture over Saudi Arabia and influences of IOD and ENSO. *Monthly Weather Review*, *134*(2), 598–617. https://doi.org/10.1175/MWR3085.1

Croitoru, A.-E., & Piticar, A. (2012). Changes in daily extreme temperatures in the extra-Carpathians regions of Romania. *International Journal of Climatology*, *33*(8), 1987–2001. https://doi.org/10.1002/joc.3567

Cullen, H. M., Kaplan, A., Arkin, P. A., & Demenocal, P. B. (2002). Impact of the North Atlantic oscillation on Middle Eastern climate and streamflow. *Climatic Change*, *55*(3), 315–338. https://doi.org/10.1023/A:1020518305517

del Río, S., Anjum Iqbal, M., Cano-Ortiz, A., Herrero, L., Hassan, A., & Penas, A. (2013). Recent mean temperature trends in Pakistan and links with teleconnection patterns. *International Journal of Climatology*, *33*(2), 277–290. https://doi.org/10.1002/joc.3423

Dogar, M. M. (2018). Impact of tropical volcanic eruptions on Hadley circulation using a high-resolution AGCM. *Current Science*, *114*(6), 1284–1294.

Dogar, M. M., Kucharski, F., & Azharuddin, S. (2017). Study of the global and regional climatic impacts of ENSO magnitude using SPEEDY AGCM. *Journal of Earth System Science*, *126*(2), 30. https://doi.org/10.1007/s12040-017-0804-4

Dogar, M. M., Kucharski, F., Sato, T., Mehmood, S., Ali, S., Gong, Z., et al. (2018). Towards understanding the global and regional climatic impacts of Modoki magnitude. *Global and Planetary Change*, *172*, 223–241.

Dogar, M. M., Stenchikov, G., Osipov, S., Wyman, B., & Zhao, M. (2017). Sensitivity of the regional climate in the Middle East and North Africa to volcanic perturbations. *Journal of Geophysical Research: Atmospheres*, *122*, 1–27. https://doi.org/10.1002/2017JD026783

Driscoll, S., Bozzo, A., Gray, L. J., Robock, A., & Stenchikov, G. (2012). Coupled Model Intercomparison Project 5 (CMIP5) simulations of climate following volcanic eruptions. *Journal of Geophysical Research*, *117*, D17105. https://doi.org/10.1029/2012JD017607

El-Samra, R., Bou-Zeid, E., Bangalath, H. K., Stenchikov, G., & El-Fadel, M. (2018). Seasonal and regional patterns of future temperature extremes: High-resolution dynamic downscaling over a complex terrain. *Journal of Geophysical Research: Atmospheres*, *123*, 6669–6689. https://doi.org/10.1029/2017JD027500

Flaounas, E., Janicot, S., Bastin, S., Roca, R., & Mohino, E. (2012). The role of the Indian monsoon onset in the West African monsoon onset: Observations and AGCM nudged simulations. *Climate Dynamics*, *38*(5–6), 965–983. https://doi.org/10.1007/s00382-011-1045-x

Freidenreich, S. M., & Ramaswamy, V. (1999). A new multiple-band solar radiative parameterization for general circulation models. *Journal of Geophysical Research*, *104*(D24), 31389–31409. https://doi.org/10.1029/1999JD900456

Ghasemi, A. R., & Khalili, D. (2008). The effect of the North Sea-Caspian pattern (NCP) on winter temperatures in Iran. *Theoretical and Applied Climatology*, *92*(1–2), 59–74. https://doi.org/10.1007/s00704-007-0309-1

Gujarati, D. N. (2009). *Basic econometrics*. New York: Tata McGraw-Hill Education.

Hansen, J., Ruedy, R., Sato, M., & Lo, K. (2010). Global surface temperature change. *Reviews of Geophysics*, *48*, RG4004. https://doi.org/10.1029/2010RG000345

Haywood, J. M., Jones, A., Bellouin, N., & Stephenson, D. (2013). Asymmetric forcing from stratospheric aerosols impacts Sahelian rainfall. *Nature Climate Change*, *3*, 660–665. https://doi.org/10.1038/nclimate1857

Horowitz, L. W., Walters, S., Mauzerall, D. L., Emmons, L. K., Rasch, P. J., Granier, C., et al. (2003). A global simulation of tropospheric ozone and related tracers: Description and evaluation of MOZART, version 2. *Journal of Geophysical Research*, *108*(D24), 4784. https://doi.org/10.1029/2002JD002853

Hurrell, J. W. (1995). Decadal trends in the North Atlantic oscillation: Regional temperatures and precipitation. *Science*, *269*(5224), 676–679. https://doi.org/10.1126/science.269.5224.676

Hurrell, J. W., & Deser, C. (2010). North Atlantic climate variability: The role of the North Atlantic oscillation. *Journal of Marine Systems*, *79*(3-4), 231–244. https://doi.org/10.1016/j.jmarsys.2009.11.002

Hurrell, J. W., Kushnir, Y., Ottersen, G., & Visbeck, M. (2003). An overview of the North Atlantic oscillation. The North Atlantic oscillation: Climatic significance and environmental impact. *Geophysical Monograph American Geophysical Union*, *134*, 1–35.

Iles, C., & Hegerl, G. (2017). Role of the North Atlantic oscillation in decadal temperature trends. *Environmental Research Letters*, *12*(11), 114010. https://doi.org/10.1088/1748-9326/aa9152

Iqbal, M., Hameed, S., & Khan, F. (2013). Influence of Azores high pressure on Middle Eastern rainfall. *Theoretical and Applied Climatology*, *111*(1–2), 211–221.

Joseph, R., & Zeng, N. (2011). Seasonally modulated tropical drought induced by volcanic aerosol. *Journal of Climate*, *24*(8), 2045–2060. https://doi.org/10.1175/2009JCLI3170.1

Klein, S. A., Soden, B. J., & Lau, N. C. (1999). Remote sea surface temperature variations during ENSO: Evidence for a tropical atmospheric bridge. *Journal of Climate*, *12*, 917–932.

Krichak, S., Kishcha, P., & Alpert, P. (2002). Decadal trends of main Eurasian oscillations and the Eastern Mediterranean precipitation. *Theoretical and Applied Climatology*, *72*(3–4), 209–220. https://doi.org/10.1007/s007040200021

Krishna, L. V. (2014). Long term temperature trends in four different climatic zones of Saudi Arabia. *International Journal of Applied*, *4*(5).

Kucharski, F., Kang, I.-S., Straus, D., & King, M. P. (2010). Teleconnections in the atmosphere and oceans. *Bulletin of the American Meteorological Society*, *91*(3), 381–383. https://doi.org/10.1175/2009BAMS2834.1

Kumar, K. N., Ouarda, T. B., Sandeep, S., & Ajayamohan, R. S. (2016). Wintertime precipitation variability over the Arabian Peninsula and its relationship with ENSO in the CAM4 simulations. *Climate Dynamics*, *47*(7–8), 2443–2454. https://doi.org/10.1007/s00382-016-2973-2

Kutiel, H., & Benaroch, Y. (2002). North Sea Caspian Pattern (NCP) - An upper level atmospheric teleconnection affecting the eastern Mediterranean: Identification and definition. *Theoretical and Applied Climatology*, *71*, 17–28.

Kutiel, H., Maheras, P., Türkeş, M., & Paz, S. (2002). North Sea-Caspian Pattern (NCP)—An upper level atmospheric teleconnection affecting the eastern Mediterranean—Implications on the regional climate. *Theoretical and Applied Climatology*, *72*(3–4), 173–192. https://doi.org/10.1007/s00704-002-0674-8

Lim, Y.-K. (2015). The East Atlantic/West Russia (EA/WR) teleconnection in the North Atlantic: Climate impact and relation to Rossby wave propagation. *Climate Dynamics*, *44*(11–12), 3211–3222. https://doi.org/10.1007/s00382-014-2381-4

Liu, F., Chai, J., Wang, B., Liu, J., Zhang, X., & Wang, Z. (2016). Global monsoon precipitation responses to large volcanic eruptions. *Scientific Reports*, *6*, 1–11.

Malyshev, S., Shevliakova, E., Stouffer, R. J., & Pacala, S. W. (2015). Contrasting local vs. regional effects of land-use-change induced heterogeneity on historical climate: Analysis with the GFDL Earth System Model. *Journal of Climate*, *28*(13), https://doi.org/10.1175/JCLI-D-14-00586.1

Moorthi, S., & Suarez, M. J. (1992). Relaxed Arakawa-Schubert. A parameterization of moist convection for general circulation models. *Monthly Weather Review*, *120*(6), 978–1002. https://doi.org/10.1175/1520-0493(1992)120<0978:RASAPO>2.0.CO;2

Neelin, J. D., Battisti, D. S., Hirst, A. C., Jin, F. F., Wakata, Y., Yamagata, T., & Zebiak, S. E. (1998). ENSO theory. *Journal of Geophysical Research*, *103*(C7), 14261–14290. https://doi.org/10.1029/97JC03424

Oman, L., Robock, A., Stenchikov, G. L., & Thordarson, T. (2006). High-latitude eruptions cast shadow over the African monsoon and the flow of the Nile. *Geophysical Research Letters*, *33*, L18711. https://doi.org/10.1029/2006GL027665

Osipov, S., Dogar, M., & Stenchikov, G. (2016). Study of regional volcanic impact on the Middle East and North Africa using high-resolution global and regional models, paper presented at EGU general assembly conference abstracts, April 01, 2016.

Parthasarathy, B. (1995). *Monthly and seasonal rainfall series for all-India homogeneous regions and meteorological subdivisions, 1871–1994*, (p. 113). Pune, India: Indian Institute of Tropical Meteorology.

Parthasarathy, B., Munot, A., & Kothawale, D. (1994). All-India monthly and seasonal rainfall series: 1871–1993. *Theoretical and Applied Climatology*, *49*(4), 217–224. https://doi.org/10.1007/BF00867461

Preethi, B., Sabin, T., Adedoyin, J., & Ashok, K. (2015). Impacts of the ENSO Modoki and other tropical indo-Pacific climate-drivers on African rainfall. *Scientific Reports*, *5*(1). https://doi.org/10.1038/srep16653

Putman, W. M., & Lin, S.-J. (2007). Finite-volume transport on various cubed-sphere grids. *Journal of Computational Physics*, *227*(1), 55–78. https://doi.org/10.1016/j.jcp.2007.07.022

Ramachandran, S., Ramaswamy, V., Stenchikov, G. L., & Robock, A. (2000). Radiative impact of the Mount Pinatubo volcanic eruption: Lower stratospheric response. *Journal of Geophysical Research*, *105*(D19), 24409–24429. https://doi.org/10.1029/2000JD900355

Randel, W. J. (2010). Variability and trends in stratospheric temperature and water vapor, the stratosphere: Dynamics, transport and chemistry, 60th.

Rayner, N., Parker, D. E., Horton, E., Folland, C., Alexander, L., Rowell, D., et al. (2003). Global analyses of sea surface temperature, sea ice, and night marine air temperature since the late nineteenth century. *Journal of Geophysical Research*, *108*(D14), 4407. https://doi.org/10.1029/2002JD002670

Rodwell, M. J., & Hoskins, B. J. (1996). Monsoons and the dynamics of deserts. *Quarterly Journal of the Royal Meteorological Society*, *122*(534), 1385–1404. https://doi.org/10.1002/qj.49712253408

Sandeep, S., & Ajayamohan, R. S. (2018). Modulation of winter precipitation dynamics over the Arabian Gulf by ENSO. *Journal of Geophysical Research: Atmospheres*, *123*, 198–210. https://doi.org/10.1002/2017JD027263

Santer, B. D., Wigley, T., Boyle, J., Gaffen, D. J., Hnilo, J., Nychka, D., et al. (2000). Statistical significance of trends and trend differences in layer-average atmospheric temperature time series. *Journal of Geophysical Research*, *105*(D6), 7337–7356. https://doi.org/10.1029/1999JD901105

Sato, M., Hansen, J. E., McCormick, M. P., & Pollack, J. B. (1993). Stratospheric aerosol optical depths, 1850–1990. *Journal of Geophysical Research*, *98*(D12), 22,987–22,994. https://doi.org/10.1029/93JD02553

Schwarzkopf, M. D., & Ramaswamy, V. (1999). Radiative effects of CH4, N2O, halocarbons and the foreign-broadened H2O continuum: A GCM experiment. *Journal of Geophysical Research*, *104*(D8), 9467–9488. https://doi.org/10.1029/1999JD900003

Stenchikov, G., & Dogar, M. (2012). Regional climate response to volcanic radiative forcing in Middle East and North Africa. In EGU General Assembly Conference Abstracts (Vol. 14, p. 6373).

Stenchikov, G., Hamilton, K., Stouffer, R. J., Robock, A., Ramaswamy, V., Santer, B., & Graf, H. F. (2006). Arctic oscillation response to volcanic eruptions in the IPCC AR4 climate models. *Journal of Geophysical Research*, *111*, D07107. https://doi.org/10.1029/2005JD006286

Sultan, B., & Janicot, S. (2000). Abrupt shift of the ITCZ over West Africa and intra-seasonal variability. *Geophysical Research Letters*, *27*(20), 3353–3356. https://doi.org/10.1029/1999GL011285

Taylor, K. E., Stouffer, R. J., & Meehl, G. A. (2009). *A Summary of the CMIP5 Experiment Design* (p. 13).

Taylor, K. E., Stouffer, R. J., & Meehl, G. A. (2012). An overview of CMIP5 and the experiment design. *Bulletin of the American Meteorological Society*, *93*(4), 485–498.

Timmermann, A., Oberhuber, J., Bacher, A., Esch, M., Latif, M., & Roeckner, E. (1999). Increased El Nino frequency in a climate model forced by future greenhouse warming. *Nature*, *398*(6729), 694–697. https://doi.org/10.1038/19505

Trenberth, K. E., Branstator, G. W., Karoly, D., Kumar, A., Lau, N. C., & Ropelewski, C. (1998). Progress during TOGA in understanding and modeling global teleconnections associated with tropical sea surface temperatures. *Journal of Geophysical Research*, *103*(C7), 14,291–14,324. https://doi.org/10.1029/97JC01444

Trenberth, K. E., & Caron, J. M. (2000). The southern oscillation revisited: Sea level pressure, surface temperatures, and precipitation. *Journal of Climate*, *13*(24), 4358–4365. https://doi.org/10.1175/1520-0442(2000)013<4358:TSORSL>2.0.CO;2

Trenberth, K. E., & Dai, A. (2007). Effects of Mount Pinatubo volcanic eruption on the hydrological cycle as an analog of geoengineering. *Geophysical Research Letters*, *34*, L15702. https://doi.org/10.1029/2007GL030524

van Loon, H., & Rogers, J. C. (1978). The seesaw in winter temperatures between Greenland and northern Europe. Part I: General description. *Monthly Weather Review*, *106*(3), 296–310. https://doi.org/10.1175/1520-0493(1978)106<0296:TSIWTB>2.0.CO;2

Wallace, J. M., & Gutzler, D. S. (1981). Teleconnections in the geopotential height field during the Northern Hemisphere winter. *Monthly Weather Review*, *109*(4), 784–812. https://doi.org/10.1175/1520-0493(1981)109<0784:TITGHF>2.0.CO;2

Wang, C. (2002). Atmospheric circulation cells associated with the El Niño-Southern Oscillation. *Journal of Climate*, *15*, 399–419.

Wanner, H., Brönnimann, S., Casty, C., Gyalistras, D., Luterbacher, J., Schmutz, C., et al. (2001). North Atlantic oscillation—Concepts and studies. *Surveys in Geophysics*, *22*(4), 321–381. https://doi.org/10.1023/A:1014217317898

Wegmann, M., Brönnimann, S., Bhend, J., Franke, J., Folini, D., Wild, M., & Luterbacher, J. (2014). Volcanic influence on European summer precipitation through monsoons: Possible cause for "years without summer". *Journal of Climate*, *27*(10), 3683–3691. https://doi.org/10.1175/JCLI-D-13-00524.1

Yu, R., & Zhou, T. (2004). Impacts of winter-NAO on March cooling trends over subtropical Eurasia continent in the recent half century. *Geophysical Research Letters*, *31*, L12204. https://doi.org/10.1029/2004GL019814

Zhang, X., Aguilar, E., Sensoy, S., Melkonyan, H., Tagiyeva, U., Ahmed, N., et al. (2005). Trends in Middle East climate extreme indices from 1950 to 2003. *Journal of Geophysical Research*, *110*, D22104. https://doi.org/10.1029/2005JD006181

Zhao, M., Held, I. M., Lin, S.-J., & Vecchi, G. A. (2009). Simulations of global hurricane climatology, interannual variability, and response to global warming using a 50-km resolution GCM. *Journal of Climate*, *22*(24), 6653–6678. https://doi.org/10.1175/2009JCLI3049.1